Motor unit localization using high-density surface EMG

Jonathan Lundsberg

Lund, 2019

Master´s Thesis in
Biomedical engineering

Supervisor: Nebojsa Malesevic

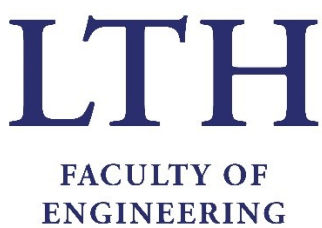

Department of Biomedical Engineering

Abstract

Localization of muscle motor units (MU) using surface electromyography (sEMG) is of interest in areas including neurology, rehabilitation and prosthetic control. The aim of the thesis is to describe a method for MU localization using high-density sEMG (HDsEMG) and verify the method using simultaneous intramuscular EMG (iEMG) recordings. Based on previous work by Roeleveld et al, two conduction models for MU localization are described. The models are analytical volume conductors implemented in MATLAB. Simultaneous iEMG (wire electrodes) and HDsEMG (8x8 electrode array) recordings from the forearm were used. EMG decomposition provided individual motor unit action potential (MUAP) trains. Using MUAP trains, the resulting surface potential distribution from individual MU firings was used to estimate MU depth. By matching MUs from iEMG and HDsEMG decomposition, the models for depth estimation were calibrated. Three MUs with known depth in the flexor digitorum profundus, abductor pollicis longus and extensor pollicis longus muscles were used. Conclusions could not be drawn on the values for signal attenuation in the models due to high variance between the MUs. The direction of the results however supported the underlying theory. More MUs are required to create reliable models. Finding matching MUs in iEMG and sEMG was difficult, but there are many ways to improve the method relating to both recording and depth estimation.

Foreword

This master thesis work began in February 2019 and finished in November 2019. It was conducted under the supervision of Nebojsa Malesevic at the department of Biomedical Engineering at Lund University, Faculty of Engineering. The topic spawned from a discussion with Christian Antfolk and Nebojsa in late 2018.

I would like to thank Christian for the opportunity to work on this project which has been both challenging and rewarding. I would like to thank Nebojsa for spending his time helping and supporting me in this project, where many enlightening and intriguing discussions helped me grasp the task at hand. And for providing the opportunity for me to bring a part of this project to Medicinteknikdagarna 2019, which is an experience I will not forget.

Table of Contents

Abbreviations

MU	Motor unit
MUAP	Motor unit action potential
EMG	Electromyography
iEMG	Intramuscular electromyography
sEMG	Surface electromyography
HDsEMG	High-density surface electromyography
FWHM	Full width at half maximum

Introduction

The source of the problem

Localization of individual motor units (MUs) in a muscle using surface electromyography (sEMG) is of interest in several research areas, including neurology, rehabilitation and prosthetic control. It is a complex problem, with limited studies addressing the topic. The task can be split into two parts. Firstly, we want to distinguish a single source, a motor unit, from a sea of active motor units during muscle contraction. We then want a model of the propagating signal, which can be used to locate the source inside the body, using the resulting surface signal alone (Figure 1). In most cases, there can be hundreds of MU firings every second, both above and below the one we are looking for. And to make it just a bit harder, sEMG recordings are incredibly noisy. The first part of the problem is tackled using software with decomposition algorithms. The models used for source localization are based on previous work by Roeleveld et al (1) and will be described in detail.

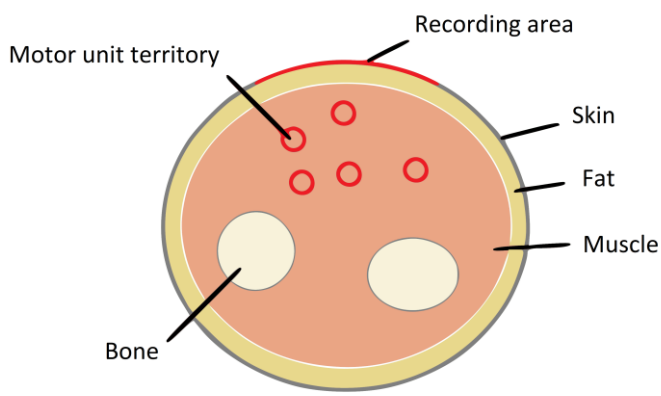

Figure 1. Schematic of a cross section of the upper forearm.

Purpose and disposition

The aim of this master thesis project is to present and describe a viable model for localization of MUs using sEMG. Before diving into the method, some background will be given to the EMG signal, some underlying

anatomy, and why it's a problem worth solving. The method section is a step-by-step description. This includes the recording setup, the software used for signal decomposition, and importantly a thorough explanation of two models used for depth estimation. After a short section of results, a discussion on the models, the results, shortcomings and areas for improvements will conclude the report. Additionally, appendices of scripts used in MATLAB are also included.

Background

From neuron to electrode

EMG recordings are based on the electrical nature of neuromuscular activity. Much like the neurons which initiate muscle contractions, each muscle fibre conducts an electric potential along its membrane. A single unit, consisting of a neuron and several muscle fibres, is called a motor unit (MU). The incoming action potential from the motor neuron is comparatively weak and is not very useful for our purpose. The resulting action potential in the muscle fibers however is much stronger and is the basis for EMG recordings. The currents generated by MUs can be picked up with electrodes, either invasively or non-invasively. Non-invasive electrodes are placed on the skin and called surface EMG (sEMG). Invasive electrodes, which can be needle or wire electrodes, are placed inside the muscle and called intramuscular EMG (iEMG). A high-density surface electrode array (HDsEMG) is used in this project, which gives a comprehensive view of the surface potential over a larger area covering the muscle.

For iEMG, the MUs closest to the electrode are relatively distinct and can often be identified in the raw signal (Figure 2). This is great for recording individual MUs but since it is an invasive recording it has many drawbacks. Penetrating the skin carries a risk of infection, it can cause discomfort for the subject, and it may disrupt or damage the surrounding tissues. Surface EMG avoids these drawbacks, however the signal is more complicated. The raw signal is more of a compound signal of the activity of all MUs in the area. Meaning that many MUs are superimposed on top of each other,

making it hard to differentiate between them. The electrode is further from the source and is largely affected by the surrounding anatomy and physiology, i.e. the signal traverses various tissues with differing conductive qualities to reach the skin surface.

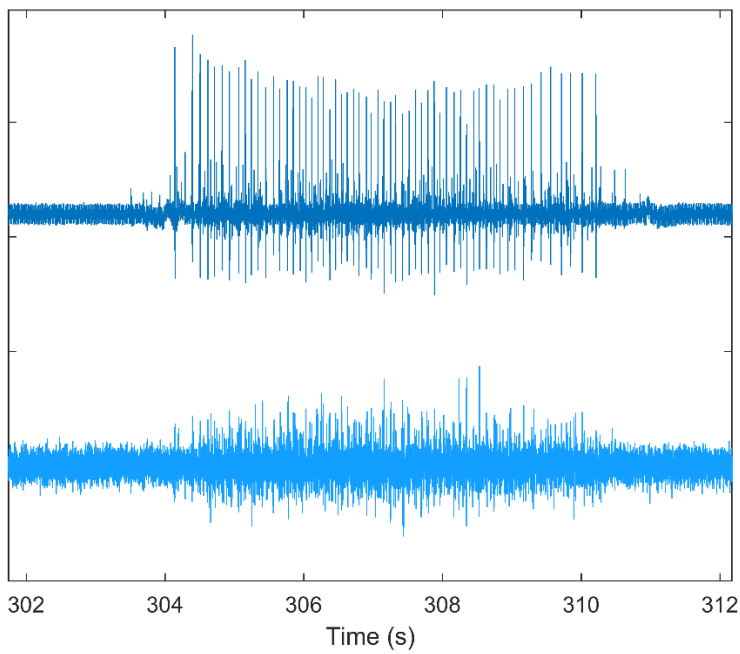

Figure 2. 10 seconds of intramuscular EMG (top) and surface EMG (bottom). The sEMG signal strength is amplified.

The underlying biology

The EMG signal produced by groups of muscle fibers, is initiated by specific motor neurons located in the brainstem and the spinal cord. A motor neuron conducts a signal in the form of action potentials through its axon all the way to the muscle. An action potential is the depolarization of the plasma membrane which travels throughout the cell. Ion-channels open successively from the neuron cell body to the end of the axon. It's an all or nothing signal, which means that every action potential will fully depolarize the membrane as it travels. Each action potential therefore has the same strength and shape as the next (Figure 3).

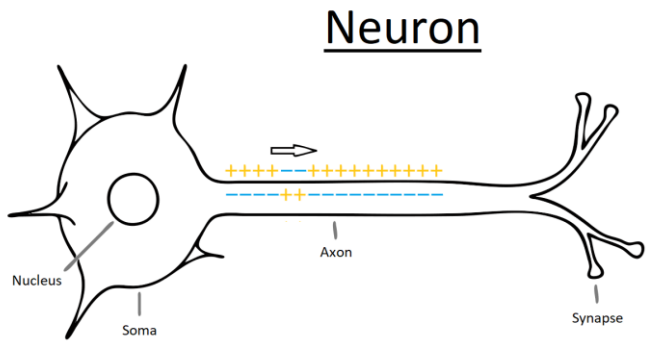

Figure 3. Schematic of a neuron and the principals of an action potential.

At the muscle, the axon branches out to several muscle fibers. The amount of fibers the motor neuron innervates varies largely between muscles. Each muscle fiber is innervated at a part of its plasma membrane called the motor end plate. An axon terminal and the motor end plate make up the neuromuscular junction (2). The motor end plate only receives a signal from a single motor neuron. A motor neuron and the fibers it innervates is defined as a single motor unit. Although each motor unit is distinct, the positions of the fibers are often spread, causing motor units to somewhat overlap with each other (Figure 4).

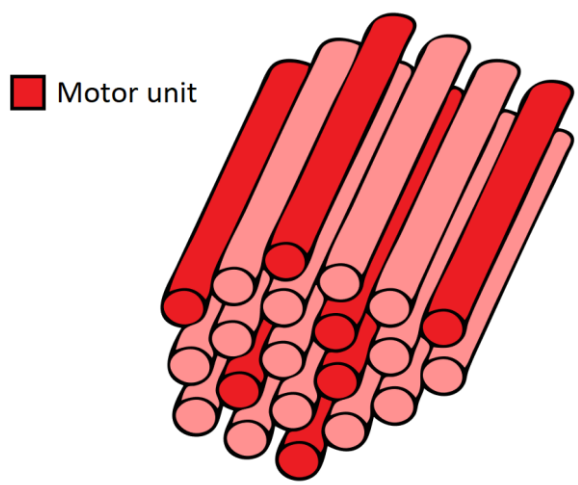

Figure 4. Schematic of several muscle fibers. The fibers of a single motor unit (red) are spread out.

Starting at the motor end plate, which is most often located near the center of a muscle fiber, the action potential spreads to both ends of the fiber. It takes time for the action potential to cover the entire fiber, which means the recorded EMG signal is spread out in both space and time. Fibers vary in length and can be as long as the muscle itself. Some are shorter and attached at an angle to the muscles longitudinal axis. The direction of the fibers also needs to be taken into account since the conductivity in a muscle is higher along the fibers than in the perpendicular plane (2)(3).

Acting in unison, the fibers of a MU together create a strong enough signal that can traverse the body to the skin surface to be recorded. It passes through the muscle itself, connective tissue, fat and skin. These tissues are not uniformly distributed which together with other irregularities, like blood vessels and bone, makes it hard to create a realistic model. There is normally a considerable layer of fat between the muscles and the skin which gives 3 distinct layers to consider; muscle, fat and skin. The skin is incredibly thin in comparison but is still the source of highest impedance. The thickness of the fat layer varies from person to person as well as from area to area. The amount of muscle tissue the signal passes through depends on the depth of the MU.

Utilities of motor unit localization

Localization of specific motor units is useful for several areas. Two clear examples are related to prosthetic control and rehabilitation. MU localization can improve the ability to distinguish different muscle activations to improve prosthetic control. For rehabilitation following motor impairment, studying MU activity can help define the effectiveness of rehabilitation treatments.

Prosthetic control using surface EMG have many approaches. Commonly used is the EMG amplitude for control of one degree of freedom at a time (4). Control schemes utilizing pattern recognition and artificial neural networks are also being developed (5)(6). However, many prosthetic devices suffer from high rejection rates, which in part is due to non-intuitive control. More intuitive control may be found by taking into account the underlying process of EMG signal generation. Using motor unit discharge

timings is an alternative which is more directly connected to the signals from our nervous system (7). With additional localization of MUs, a more physiologically accurate method for prosthetic control can be developed. Such a method could potentially map the surface EMG signal proportionally to individual muscles, allowing for natural and intuitive control.

Every year 15 million people worldwide suffer a stroke (8). Motor impairment is a common consequence of stroke, which affects 80% of patients, making it a leading cause of adult disability in most countries (9)(10). Motor recovery is complicated and rehabilitation approaches are numerous with varying results. Comprehensive reviews on these approaches have been made in attempts to define their effectiveness and determine appropriate interventions (9)(10). They conclude that although some approaches are promising, there are many gaps and shortcomings in the evidence base for interventions. The clinical decisions, therefore, continue to rely on individual therapists. Recommendations are made for research to much more clearly define the effect of specific rehabilitation interventions and to better understand the underlying mechanisms. Monitoring MU activity over time may provide a measure for this. By mapping MU activity to muscles of interest, we can study the recovery of motor units during rehabilitation treatments, e.g. to measure MU recovery rate (Figure 5). This could ultimately become a tool to help inform the decisions on future rehabilitation treatments.

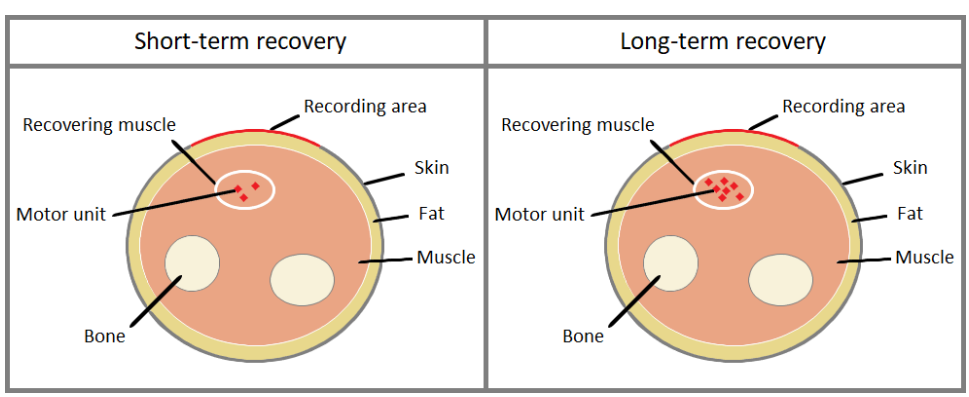

Figure 5. Illustration of MU recovery over time. With MU localization, recovery in a specific muscle or area can be studied in patients recovering from motor impairment after stroke.

Monopolar and differential configurations

When using an array of electrodes, e.g. HDsEMG, the measurements can be either monopolar or differential. In monopolar measurements each individual electrode is compared to a single reference electrode which is carefully placed at a position with a stable electric potential. Differential or bipolar measurements instead compares the potential at each electrode with the closest subsequent electrode. Noise from distant sources affect neighboring electrodes in a similar manner since they are relatively close to each other. The effects of surrounding equipment and potential crosstalk from nearby muscles therefore partially cancels out, reducing the noise level. Without a fixed reference however, the differential setup measures only relative values.

Noise becomes a larger issue for monopolar measurements since the distance between the measuring electrode and reference electrode is greater. Consequently, it carries a lower signal-to-noise ratio, even though the mean amplitude of the recording is stronger. Additionally, monopolar measurements are seemingly more complicated to perform than differential measurements due to extra considerations required for the reference electrode. Changes in potential at the reference electrode can influence the recording so the stability of the reference point needs to be considered (11)(12)(13). However analyzing monopolar recordings may be less complicated. In this thesis, the recordings used are from a differential configuration, since it was easier to set up.

Decomposition

To study an individual motor unit, it needs to be separated from the raw signal. This is a considerable challenge for sEMG due to the complexity of the signal, containing superpositions of many motor unit action potentials (MUAPs) and high levels of noise. The sEMG electrodes are far less selective than iEMG electrodes, which have commonly been used for studying motor units. Tools for decomposing single channel iEMG have been around for quite some time. Recent advances in sEMG decomposition techniques also allow for the extraction and study of single motor units from high-density electrode arrays covering a muscle (14)(15)(16). The

separation achieved through various decomposition techniques and algorithms returns individual MUAP trains, i.e. the time of each firing of individual MUs.

The increased number of channels in HDsEMG make it possible to apply component analysis methods. Originally used in the Convolution Kernal Compensation algorithm, accounting for the effects across all electrodes. The discharge timings of MUs, i.e. the MUAP trains, are represented by a series of delta functions. An unknown mixing matrix is introduced where the impulse response correspond to the action potentials of the motor units. The MUAP trains, mixing matrix and an additional vector for noise together result in the sampled signal. The inverse problem of this system is then solved (14, 17).

Decomposed MUAP trains can be used to give a comprehensive image of how a single MU firing affects the potential distribution across the skin. By averaging the raw signal from each firing, noise and distant motor units cancel out. Given enough firings, the effect of a single motor unit on the surface potential can be visualized (Figure 6).

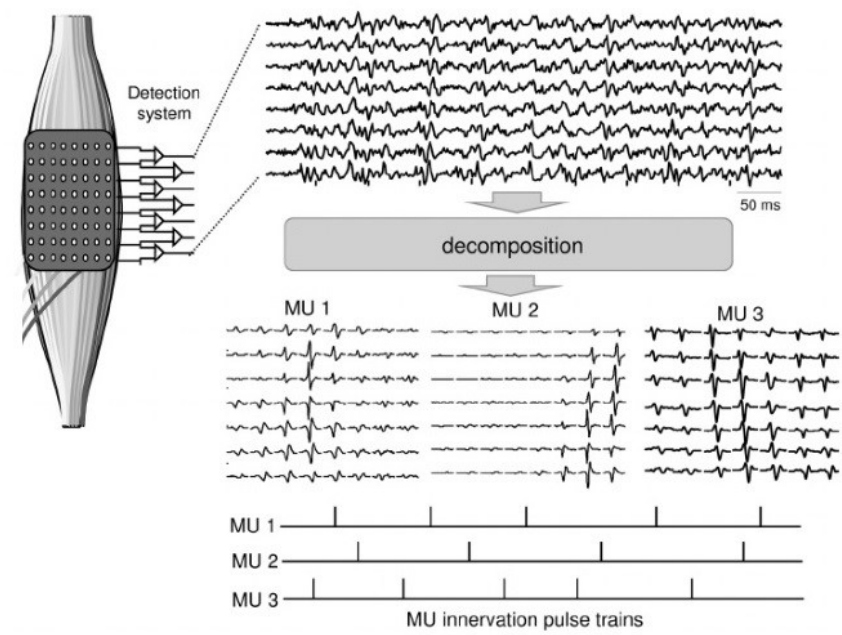

Figure 6. Illustration of the principle of HDsEMG decomposition and extraction of MU potential distributions. Image from (18).

Depth estimation of individual motor units

The potential distribution across the skin from a single MU can be used to estimate its depth, as described by Roeleveld et al (1). The idea is that with increased motor unit depth, the distance to each electrode on the skin surface becomes approximately the same and the potential will, therefore, be more uniformly distributed. In contrast, a motor unit close to the surface will be close to a few electrodes and relatively far away from others and the potential will, therefore, be much stronger at the closest electrodes with a non-uniform distribution across the skin.

Roeleveld et al (1) describe an analytical method for depth estimation from the peak potentials of electrodes perpendicular to the fiber direction over the skin. They used a basic model where the sEMG signal amplitude declines with increased radial distance to the motor unit. In that study, the authors model the body part as a single homogeneous volume conductor. In this thesis, a similar one-layer model, as well as an expanded two-layer model, are tested. The models are not sufficient on their own and require verification. In order to verify and calibrate the models, recordings with parallel iEMG and sEMG was used. The high selectivity of iEMG allows for precise knowledge of MU locations. This can then be used when estimating the depth of the same MU using sEMG.

Method

The recording setup

Several recordings of simultaneous iEMG and HDsEMG have been made at the Dept. of Biomedical Engineering, Lund University. However, only two of the datasets returned MUs after sEMG decomposition. The first dataset was recorded from the upper forearm. The HDsEMG consisted of an 8 by 8 electrode array and recording in a bipolar configuration. The HDsEMG was centered over an iEMG wire electrode inside the flexor digitorum profundus muscle (Figure 7). The depth of the iEMG electrode was approximately 1 cm and the arm circumference 28 cm.

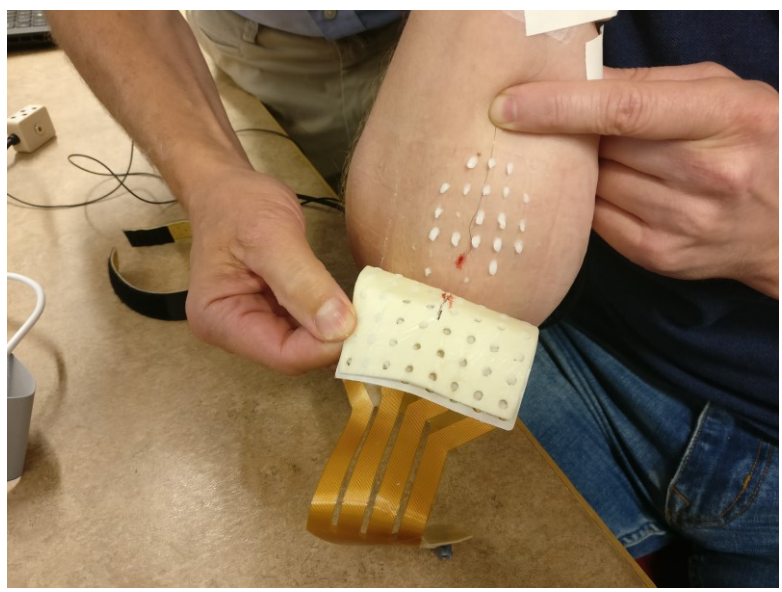

Figure 7. Image of the HDsEMG array and iEMG wire electrode on the subject's upper forearm.

The second data set was recorded from the posterior side of the lower forearm. The HDsEMG array was in a bipolar configuration. Three iEMG wire electrodes were placed in the extensor indicis proprius, abductor pollicis longus and extensor pollicis longus at 0,841 ; 0,910 and 1,58 cm depth respectively (Figure 8).

Figure 8. Image of the HDsEMG array and three iEMG wire electrodes on the subject's lower forearm.

The depth of these iEMG electrodes were precisely measured using ultrasound (Figure 9, 10 and 11). Additionally, using ultrasound, the layer of fat between the muscles and the skin was measured to approximately 0.3 cm. The arm circumference was approximately 18 cm.

Figure 9. Ultrasound measurement of the wire electrode in the extensor indicis proprius muscle. Wire depth is measured to 0,841 cm.

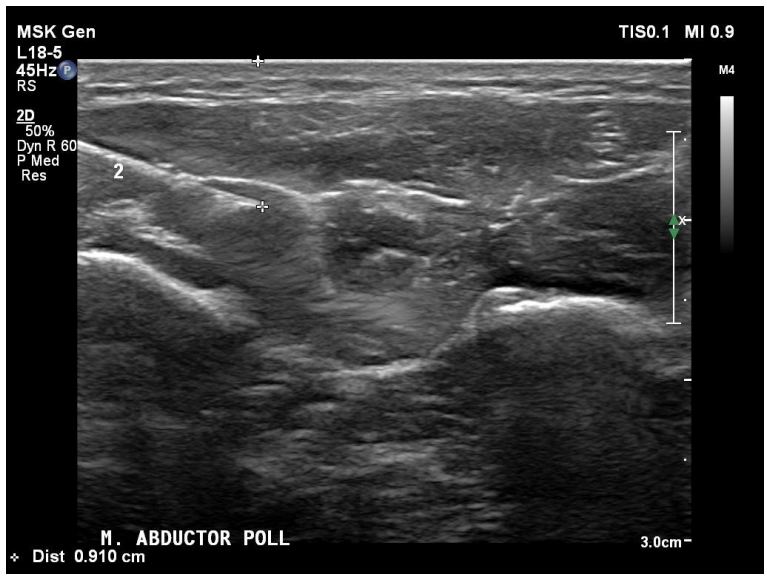

Figure 10. Ultrasound measurement of the wire electrode in the abductor pollicis longus muscle. Wire depth is measured to 0,910 cm.

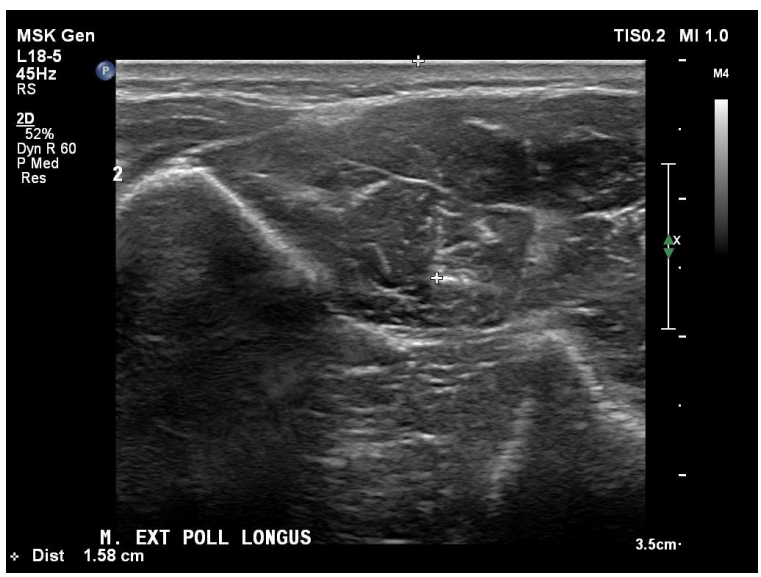

Figure 11. Ultrasound measurement of the wire electrode in the extensor pollicis longus muscle. Wire depth is measured to 1,58 cm.

The EMG datasets were recorded over the course of 30 minutes at 10240 Hz in BioLab from OT Bioelectronica. The subject followed a specific protocol, performing different isometric exercises with the hand. The force of each movement was measured and the subject would track a force in a separate LabVIEW program (Figure 12).

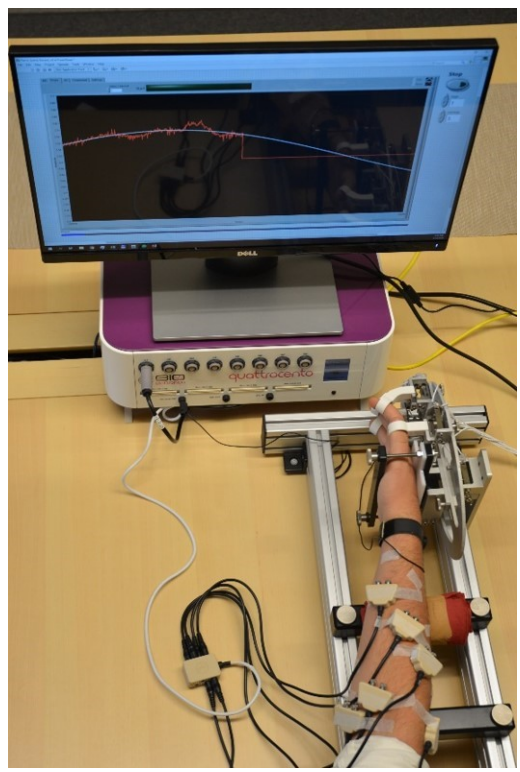

Figure 12. Image of the recording setup where the force of the subjects hand movements are measured and shown in a LabVIEW program. The subject is tracking a sine curve by regulating the force of their movement.

Surface decomposition

In order to find individual MUAP trains, the HDsEMG datasets were decomposed in BioLab. The decomposition algorithm was applied on segments, between 20-100 seconds long (Figure 13). The amount of MUAP trains returned by the algorithm varied between segments, from none up to 15 MUAP trains. The datasets and MUAP trains were then imported to MATLAB.

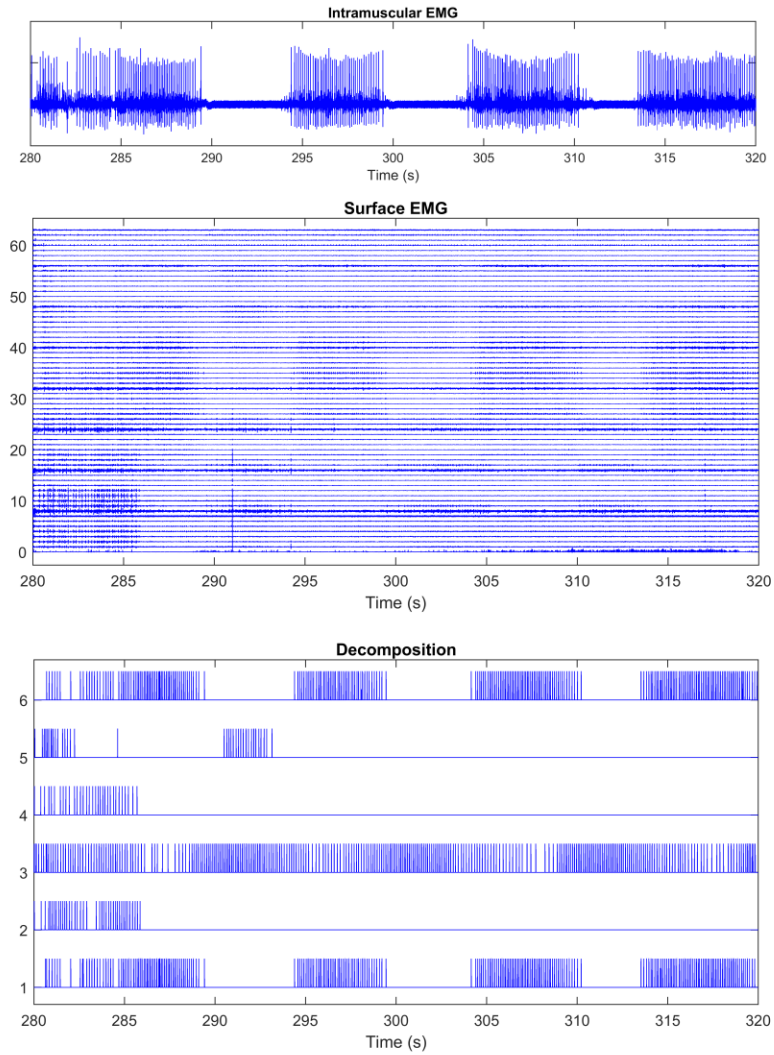

Figure 13. 40 seconds of raw intramuscular EMG (top), high-density surface EMG (middle) and individual MUAP trains from decomposition (bottom).

The matching of iEMG and MUAP trains from sEMG decomposition was done manually. Each MUAP train was plotted with the raw iEMG signal and searched for matching spikes (Figure 14-17). Since the position of the iEMG electrodes were measured using ultrasound, MUAP trains matching the iEMG recording had a known depth.

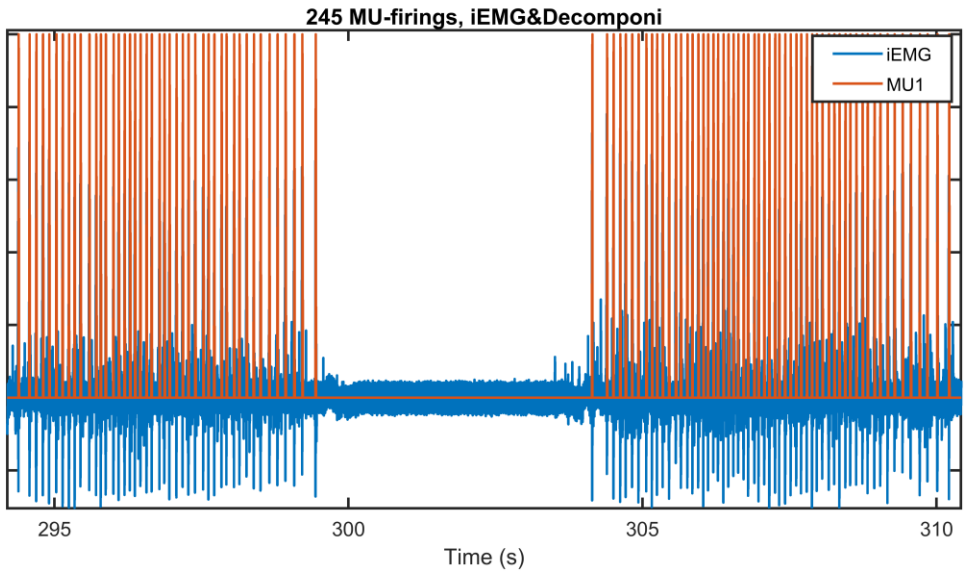

Figure 14. A section of intramuscular EMG from the flexor digitorum profundus muscle of the first dataset (blue) and a matching MUAP train from HDsEMG decomposition (red). The activity of the iEMG and the MUAP train match.

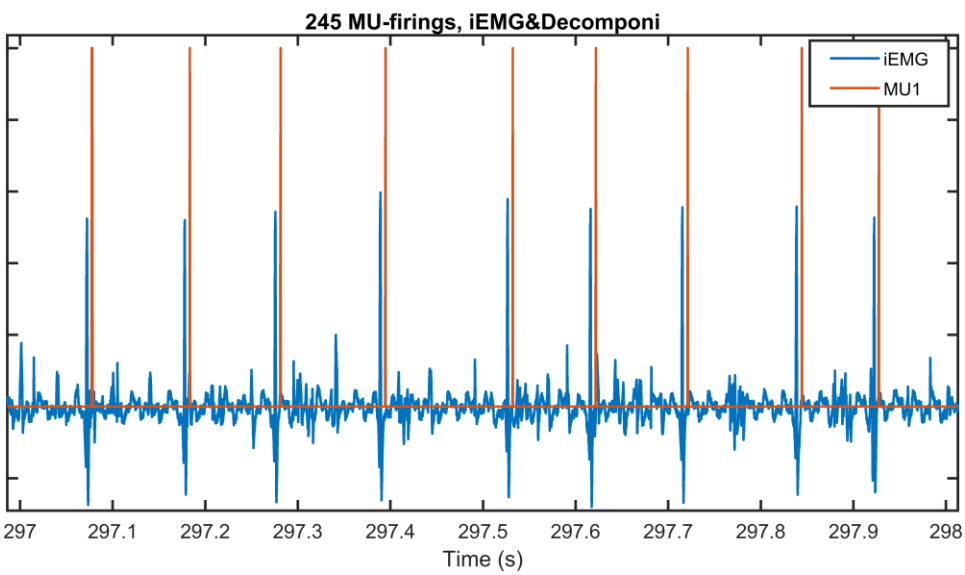

Figure 15. A section of intramuscular EMG from the flexor digitorum profundus muscle of the first dataset (blue) and a matching MUAP train from HDsEMG decomposition (red). Each firing in the MUAP train corresponds to a large peak in the iEMG signal.

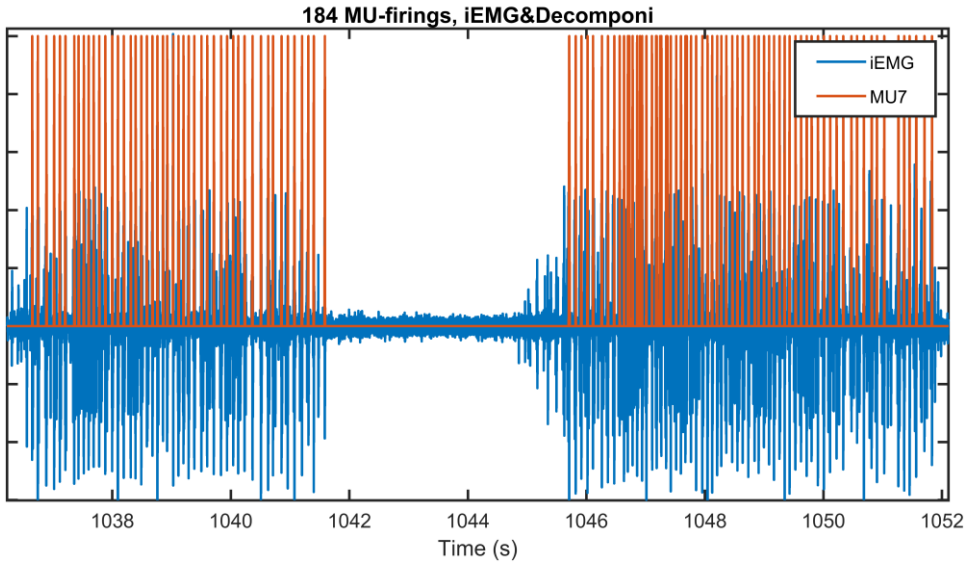

Figure 16. A section of intramuscular EMG from the abductor pollicis longus muscle of the second dataset (blue) and a matching MUAP train from HDsEMG decomposition (red). The iEMG signal is slightly messy and contains a large range of spike sizes.

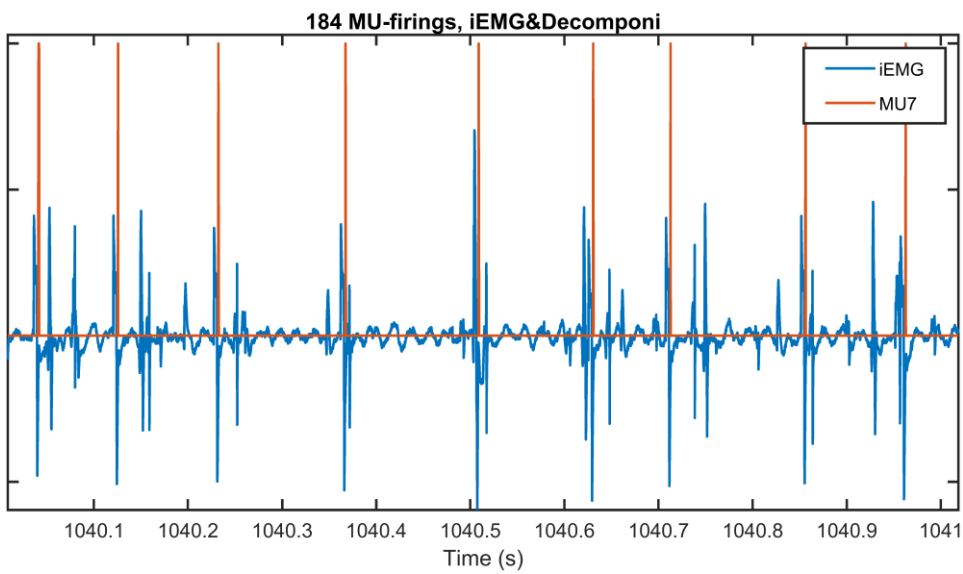

Figure 17. A section of intramuscular EMG from the abductor pollicis longus muscle of the second dataset (blue) and a matching MUAP train from HDsEMG decomposition (red). Each firing of the MUAP train corresponds to a spike in the iEMG signal. However, in contrast to the flexor digitorum profundus muscle, there are here many more spikes in the iEMG signal.

Intramuscular decomposition

Few MUAP trains from sEMG decomposition were found matching the raw iEMG. Therefore, to further calibrate the model, decomposition was also performed on the iEMG signal in the extensor pollicis longus muscle. This decomposition was done using the software Emglab, which decomposed segments of less than 100 seconds at a time. The software returned many individual MUAP trains (Figure 18), which could be used in a similar manner as MUAP trains from sEMG decomposition. The MUAP trains from intramuscular decomposition were also imported to MATLAB.

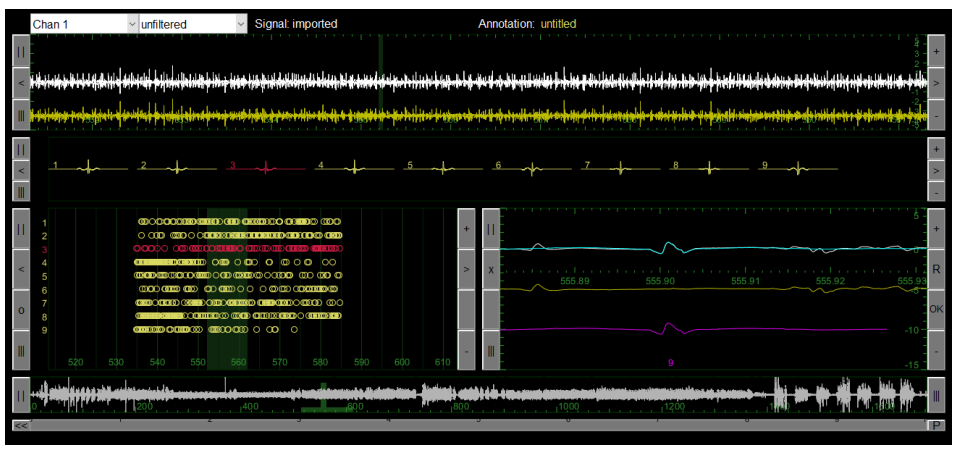

Figure 18. A segment decomposition of the iEMG electrode in the extensor pollicis longus muscle using Emglab, returning 9 MUAP trains (bottom left).

Motor units extracted from sEMG

The MUAP trains were used for depth estimation. The raw sEMG data for each firing of the MUAP train was averaged to remove noise and create a clear image of how the MU affected the surface potential (Figure 19-21).

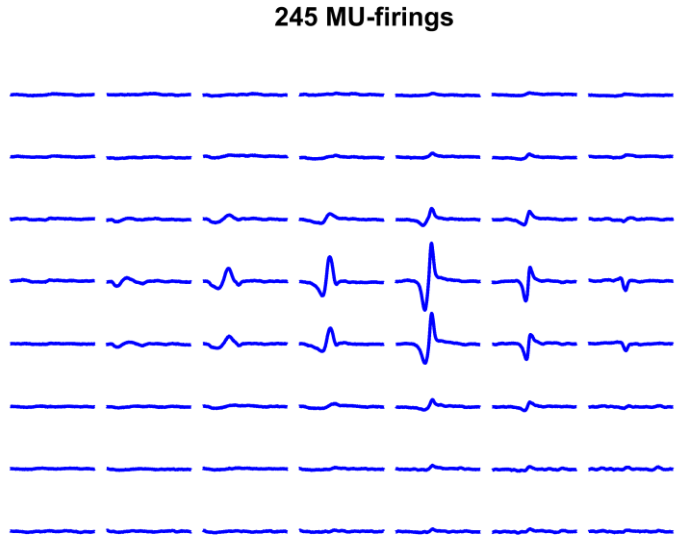

Figure 19. Extracted MU in the flexor digitorum profundus muscle. Each sEMG signal was averaged using each instance of 245 firings in a MUAP train from HDsEMG decomposition. The far right column is excluded due to the nature of the differential recording setup. The fifth column was used for depth estimation.

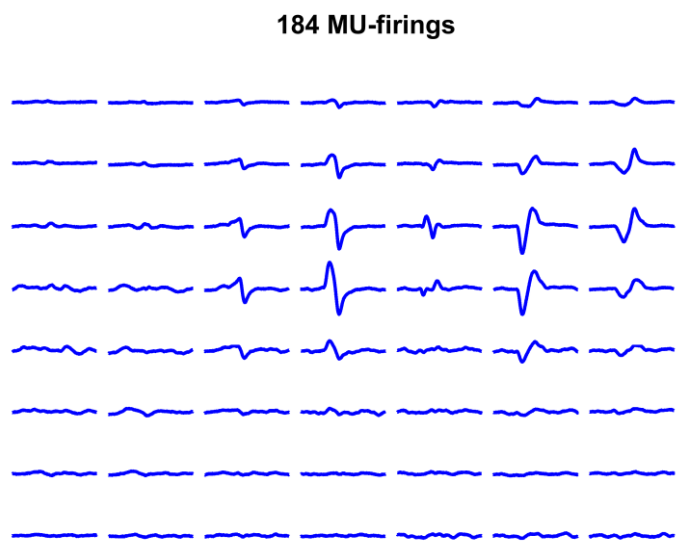

Figure 20. Extracted MU in the abductor pollicis longus muscle. Each sEMG signal was averaged using each instance of 184 firings in a MUAP train from HDsEMG decomposition. The far right column is excluded due to the nature of the differential recording setup. The trough in the fifth column is likely also due to the differential setup. The sixth column was used for depth estimation.

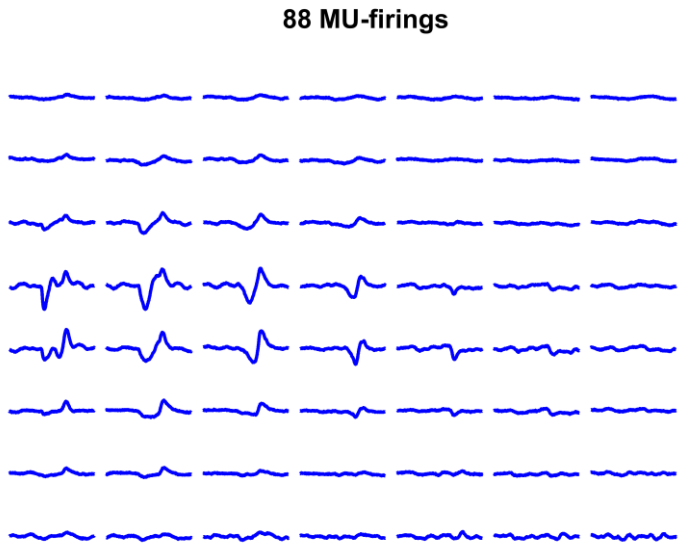

Figure 21. Extracted MU in the extensor pollicis longus muscle. Each sEMG signal was averaged using each instance of 88 firings in a MUAP train from iEMG decomposition. The far right column is excluded due to the nature of the differential recording setup. The second column was used for depth estimation.

Depth estimation

One-layer model

The first model, as described by Roeleveld et al (1), assumes a constant attenuation level of the signal from the source to the surface electrodes, i.e. a single homogeneous layer. The distance from the source to an electrode is the radial distance $r(j)$. A power function is used to describe the relation between radial distance and the surface amplitude $V(j)$, specifically for electrodes in the plane perpendicular to the muscle fiber.

$$V(j) = k \cdot \left(\frac{r(j)}{r_k}\right)^{-Q} \quad [1]$$

k is the amplitude estimate for the signal at distance r_k and Q describes the strength of signal attenuation. A higher Q means the amplitude of the signal decreases faster as it travels to the skin surface. An important thing to note is that the attenuation power affects distant electrodes more than electrodes closer to the source. This means that a lower attenuation strength results in

a more uniform distribution.

The surface signal should be strongest at the point with the shortest radial distance, which is directly above the MU. For this point $V(j) = V_{max}$ and $r(j) = d$, the MU depth. The position on the surface where the potential reaches half maximum is labeled V_F with radial distance r_F. This point is found by looking at the distribution of the signal across the skin which will be covered later. By combining the equation for V_{max} and V_F, some constants cancel out which results in

$$V_{max} = k \cdot \left(\frac{d}{r_k}\right)^{-Q}, V_F = k \cdot \left(\frac{r_F}{r_k}\right)^{-Q}$$

$$\Rightarrow \frac{V_{max}}{V_F} = \left(\frac{d}{r_F}\right)^{-Q} \Rightarrow 2 = \left(\frac{r_F}{d}\right)^{Q}$$

$$\Rightarrow r_F/d = 2^{1/Q} \qquad [2]$$

where r_F and d are unknown for each MU and Q, which we want to estimate, is constant for the entire volume.

In addition to the power function, r_F and d are also related through geometric equations. The shape is simplified to a cylindrical shape as seen in Figure 22.

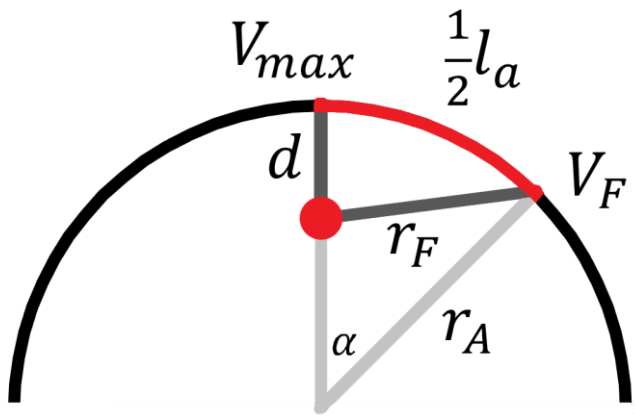

Figure 22. Schematic of the geometry of the model. The MU location is marked as the red circle.

Three points; the MU, the center of the cylinder and the surface point with half maximum amplitude, create a triangle. This triangle is subject to the cosine rule where the angle α is the angle between the lines from the center of the cylinder to V_{max} and V_F. The sides of the triangle are $(r_A - d)$ and r_A respectively and the side opposing α is r_F. We get the following,

$$a^2 = b^2 + c^2 - 2bc \cdot \cos(\alpha)$$

$$\Rightarrow r_F^2 = r_A^2 + (r_A - d)^2 - 2r_A(r_A - d)\cos(\alpha). \quad [3]$$

We then separate d^2,

$$\Rightarrow r_F^2 = d^2 - 2r_A d(1 - \cos(\alpha)) + 2r_A^2(1 - \cos(\alpha)). \quad [4]$$

Again, r_F and d are unknown for each MU, so we combine equation [2] and [4] by replacing r_F^2 with

$$r_F^2 = (2^{1/Q} \cdot d)^2.$$

This results in

$$\Rightarrow 2^{2/Q} \cdot d^2 = d^2 - 2r_A d(1 - \cos(\alpha)) + 2r_A^2(1 - \cos(\alpha))$$

$$\Rightarrow d^2(1 - 2^{2/Q}) - 2r_A d(1 - \cos(\alpha)) + 2r_A^2(1 - \cos(\alpha)) = 0.$$

We simplify the equation by introducing

$$\gamma = 1 - 2^{2/Q},$$

and extract the depth d,

$$\Rightarrow d = \frac{r_A}{\gamma}\left(\left(1 - \cos(\alpha)\right) \pm \sqrt{(1 - \cos(\alpha))^2 - 2\gamma(1 - \cos(\alpha))}\right). \quad [5]$$

The angle α depends on the surface distance between V_{max} and V_F. This distance is labeled $\frac{1}{2}l_a$, which gives the angle in radians as

$$\alpha = \frac{l_a}{2r_A}.$$

The distance $\frac{1}{2}l_a$ between V_{max} and V_F is obtained from surface potential distribution over the skin, caused by the MUAP. The surface potential distribution perpendicular to the fiber direction follows a gaussian curve.

$$f(x) = ae^{-\frac{(x-b)^2}{2c^2}}$$

Where a is the maximum amplitude, b is the horizontal offset of the maximum amplitude and c is related to the width of the gaussian curve. The full width at half maximum (FWHM) of a gaussian curve corresponds to l_a according to

$$l_a = 2\sqrt{2\ln(2)} \cdot c$$

A gaussian fit in MATLAB is applied to the peak-to-peak values of the electrodes perpendicular to the fiber direction. The column with the strongest signal is chosen manually (Figure 23).

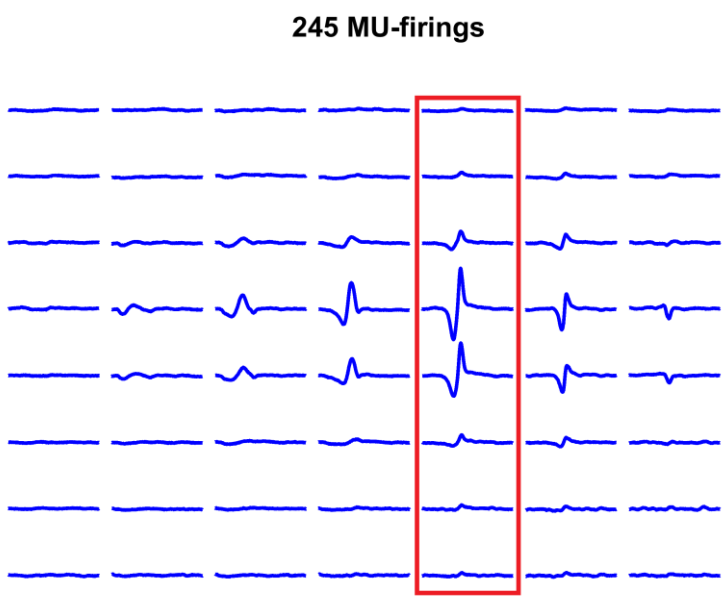

Figure 23. Extracted MU in the flexor digitorum profundus muscle. A gaussian fit is applied to the peak to peak values of the electrodes in the selected region.

The assumption for this model is that Q is constant for the entire section. In the original paper by Roeleveld et al (1), the power Q varies between 0,9 and 2,0. These values were used as starting points for the model. The depth of the MU was approximately known, and the power Q was calibrated to match the MU depth. A visualization of the MU depth was also implemented in MATLAB using the measured parameters and estimated depth.

Two-layer model

In order to expand the model to two layers, a different approach to the original power function was used. A starting amplitude, A_0 is assigned to the source, the center of the MU. It is assumed that the attenuation of the signal is constant in muscle and constant in fat respectively. As the signal traverses the muscle, perpendicular to the fiber direction, the signal amplitude is modified with an exponential function. Starting with

$$A = A_0 \cdot e^{-ax}$$

where x is the distance through muscle the signal traverses and a is the strength of signal attenuation. A larger attenuation constant again means the signal decreases faster with distance. To account for a layer of fat, which further decreases the amplitude of the signal, the equation is expanded with

$$A = A_0 \cdot e^{-ax} \cdot e^{-by} \Rightarrow A = A_0 \cdot e^{-ax-by}. \quad [6]$$

The distance through fat is y and the signal attenuation in fat is b.

In a similar manner to the one-layer model, the distribution of the signal across the skin is also important. Combining the points of maximum amplitude A_1 and half maximum A_F results in

$$A_1 = A_0 \cdot e^{-ax_1-by_1}, A_F = A_0 \cdot e^{-ax_F-by_F}$$

$$\frac{A_1}{A_F} = \frac{e^{-ax_1-by_1}}{e^{-ax_F-by_F}} \Rightarrow 2 = e^{-ax_1-by_1+ax_F+by_F}$$

$$\Rightarrow \ln(2) = -ax_1 - by_1 + ax_F + by_F$$

$$\Rightarrow \ln(2) = a(x_F - x_1) + b(y_F - y_1). \quad [7]$$

Additionally, we have

$$d = x_1 + y_1$$

$$r_F = x_F + y_F$$

The thickness of fat y_1 is measured using ultrasound. With a two-layer model however, there are too many unknown variables. In order to continue,

a few important assumptions and simplification are made. An approximation is applied where the ratio of the distances d and r_F is equivalent to the ratio of the subcomponent distances in muscle and fat respectively. I.e. since the distance r_F is greater than d, the fractions of r_F are similarly greater than the fractions of d. Which means

$\frac{r_F}{d} \approx \frac{x_F}{x_1} \approx \frac{y_F}{y_1}$.

The variables in equation [7] are replaced and expressed using r_F and d.

$$\ln(2) = -ax_1 - by_1 + ax_F + by_F$$

$$\Rightarrow \ln(2) = -ax_1 - by_1 + ax_1\frac{r_F}{d} + by_1\frac{r_F}{d}$$

$$\Rightarrow \ln(2) = ax_1\left(\frac{r_F}{d} - 1\right) + by_1\left(\frac{r_F}{d} - 1\right)$$

$$\Rightarrow \ln(2) = (ax_1 + by_1)\left(\frac{r_F}{d} - 1\right)$$

Since thickness of fat y_1 is known, this gives

$$x_1 = d - y_1$$

$$\Rightarrow \ln(2) = (a(d - y_1) + by_1)\left(\frac{r_F}{d} - 1\right) \qquad [8]$$

A simplification is made regarding the signal attenuations a and b. Conductivity is greater in muscle than in fat but measured values vary greatly. Conductivity studies (19) for the relevant frequency range (<1000 Hz) show approximately 15 times greater conductivity for muscle compared to fat. To simplify calibrating the attenuation constants, values where

$$b = a \cdot 15$$

were chosen for this model.

Just as in the one-layer model, r_F and d are also related geometrically through the cosine rule. A system of equations, consisting of equation [3] and [8], is solved using MATLAB. With precise knowledge of MU depth from ultrasound recordings, the constants for attenuation are then calibrated.

Results

Flexor digitorum profundus

From the first dataset, HDsEMG decomposition returned a MUAP train with a clear match to the iEMG signal in the flexor digitorum profundus muscle in the upper forearm. The electrode depth was approximately 1 cm, estimated without ultrasound. The arm circumference was 28 cm and the MU is shown in Figure 24. With a Gaussian fit of the peak-to-peak values of the fifth column, the FWHM of the surface distribution was estimated to

$l_a = 1{,}8$.

Using these parameters, the one-layer and two-layer models were calibrated, returning values for the attenuation constants of the models.

$Q = 2{,}9$

$a = 0{,}5$ and $b = 7{,}5$.

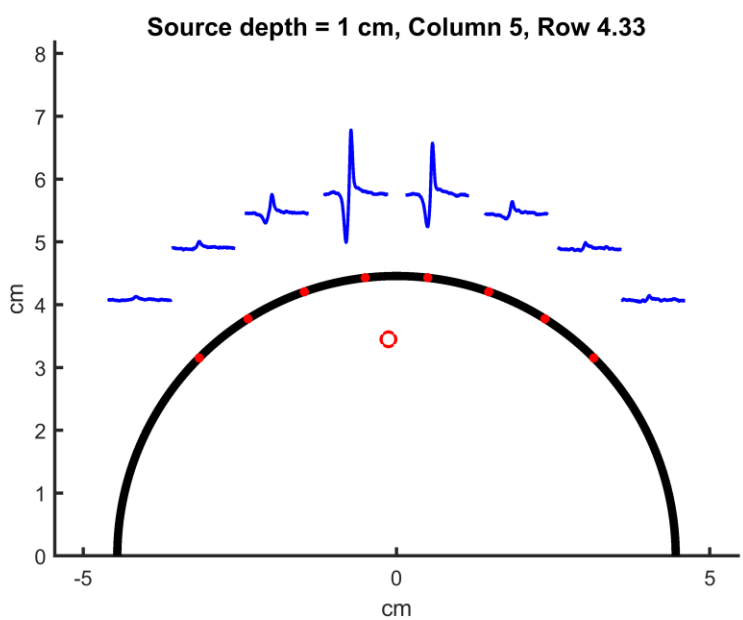

Figure 24. Visualization of the MU in the flexor digitorum profundus muscle from a cross section of the fifth column.

Abductor pollicis longus

From the second dataset, HDsEMG decomposition only returned a matching MUAP train for the iEMG signal in the abductor pollicis longus muscle in the lower forearm. The match was not as clear as in the first dataset with many additional spikes in the iEMG signal which were not covered by the MUAP train from decomposition. The electrode depth was 0,91 cm, measured using ultrasound. The arm circumference was 18 cm and the MU is shown in Figure 25. With a Gaussian fit of the peak-to-peak values of the sixth column, the FWHM of the surface distribution was estimated to

$l_a = 2{,}5$.

With these parameters, the one-layer and two-layer models were calibrated, returning values for the attenuation constants of the models.

$Q = 1{,}7$

$a = 0{,}28$ and $b = 4{,}2$.

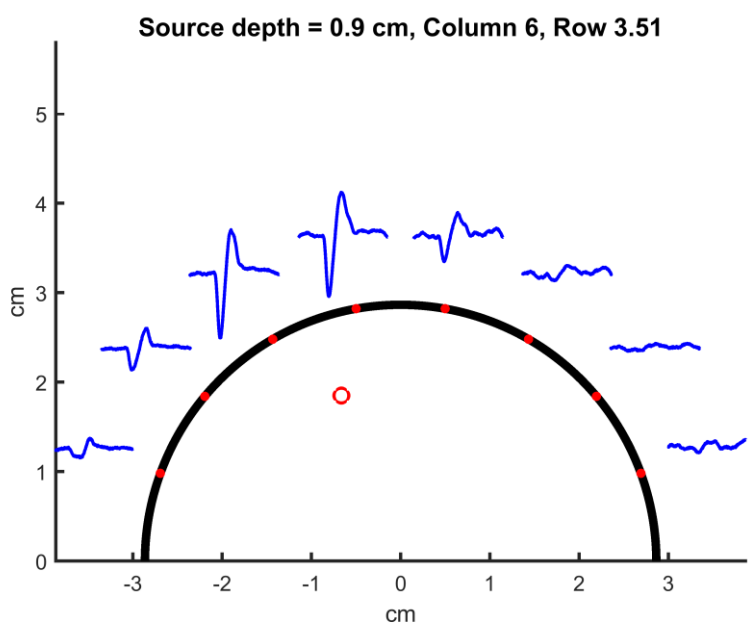

Figure 25. Visualization of the MU in the abductor pollicis longus muscle from a cross section of the sixth column.

Extensor pollicis longus

HDsEMG decomposition of the second dataset did not return MUAP trains matching the iEMG in the extensor pollicis longus nor the extensor indicis proprius. Decomposition of iEMG from the extensor pollicis longus returned several MUs. The electrode depth was 1,58 cm, measured using ultrasound. The arm circumference was 18 cm and the strongest MU is shown in figure 26. With a Gaussian fit of the peak-to-peak values of the second column of each MUAP train, the FWHM of the surface distribution was estimated between

$3{,}3 > l_a > 2{,}7$.

With these parameters, the one-layer and two-layer models were calibrated, returning a range of values for the attenuation constants of the models.

$3{,}5 < Q < 5$

$0{,}55 < a < 0{,}81$ and $8{,}25 < b < 12{,}15$.

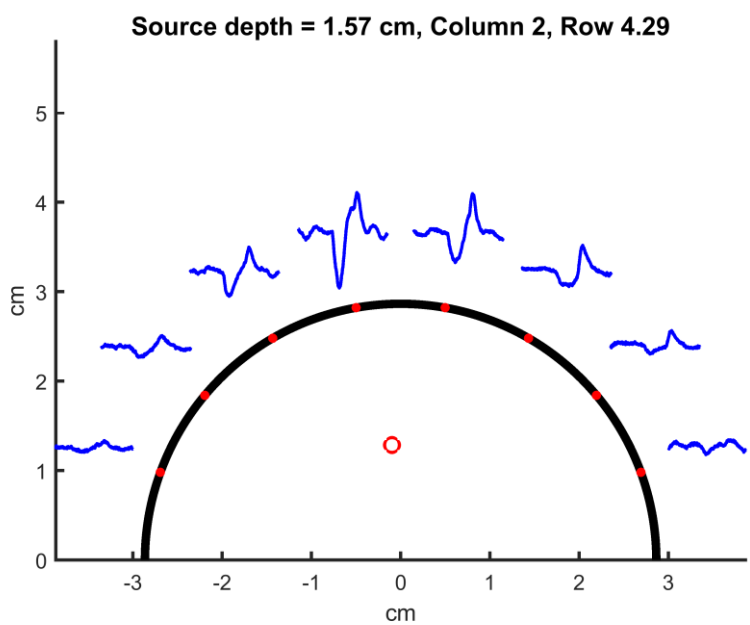

Figure 26. Visualization of the MU in the extensor pollicis longus muscle from a cross section of the second column.

The corresponding depth, FWHM and attenuation constants for both models are summarized for all three extracted motor units in table 1.

Table 1. Summary of the MUs in the flexor digitorum profundus (FDP), abductor pollicis longus (APL) and extensor pollicis longus (EPL) muscles. Several MUAP trains were used for the extensor pollicis longus which returned a range values for the FWHM of the surface distribution and attenuation constants.

	Depth	FWHM	One-layer model	Two-layer model	
	d	l_a	Q	a	b
FDP	1	1,8	2,9	0,5	7,5
APL	0,9	2,5	1,7	0,28	4,2
EPL	1,57	$3{,}3 - 2{,}7$	$3{,}5 - 5{,}0$	$0{,}55 - 0{,}81$	$8{,}25 - 12{,}15$

Discussion

The aim of this thesis was to present and describe a viable model for localization of MUs using sEMG. Although the method presented is promising, its viability is yet to be fully determined. With limited MUs to work with, it is difficult to draw strong conclusions. There is quite some variance in the resulting attenuation constants between the MUs. There are several sources of variance to account for and possible faults in the method to cover. The results show promise in some aspects however and there is much work that can be done to improve the model.

It's a good idea to first understand how the parameters of the model affect the results. As previously mentioned, a deeper MU creates a wider potential distribution on the surface and a larger FWHM l_a. Conversely however, a larger attenuation power creates a more narrow distribution and a smaller l_a. For a given distribution, i.e. the MU specific input data, changes in the models attenuation strength inversely change the resulting depth estimated for the MU. Changes in the body part circumference have an effect as well. Increasing the circumference increases the distance to the electrodes farthest away, with similar effects as changes in attenuation power.

Supporting the theory

The MU of the flexor digitorum profundus has the most narrow distribution. In comparison, the MU of the extensor pollicis longus has a clearly wider distribution. This is what was expected for a deeper MU which supports the underlying theory of the method. When instead compared to the MU of the abductor pollicis longus we again see a wider distribution, however with similar depth. This could be due to the circumference difference of the upper and lower forearm. The larger circumference around the flexor digitorum profundus should result in more narrow distributions for a given depth. If we compare the abductor pollicis longus and extensor pollicis longus MUs we see a smaller difference in distribution for a large difference in depth. As for all the MU comparisons, theory supports the direction of the results, however the details and consequently the attenuation constants still vary considerably. Therefore, with these MUs, we cannot draw conclusions on

the values of the attenuation constants for the models.

Variance

The primary source of uncertainty for the MU of the flexor digitorum profundus is the intramuscular electrode depth, since this dataset did not include ultrasound to locate the iEMG wire. If the true depth of the MU is shallower than measured, this would result in smaller attenuation constants for the models. The position of the other iEMG carry some uncertainty as well, but not nearly as much.

The extracted MU of the abductor pollicis longus (Figure 20) has a confusing shape to it which may affect the result. A trough seem to separate two peaks in the surface distribution. This is likely due to recording with a differential setup. Furthermore it is unclear how much the differential setup affects the results compared to monopolar. Although there is reduced noise, there is increased complexity when analyzing the signal. Decomposition of monopolar recordings may reveal MUs which differential decomposition does not. A monopolar setup is seemingly more optimal, especially since differential data can more easily be reconstructed from a monopolar recording.

Internal irregularities, like variation in thickness of the fat layer, blood vessels and connective tissue, could affect the results from any one MU, which is difficult to account for. Varying shapes of body parts may affect the result as well. The models assume the shape to be a perfect cylinder, which may be a good estimation for larger limbs but perhaps insufficient for the lower forearm. The curvature around the lower forearm varies significantly which affects the distance from the MU to each electrode. A larger body part, like the thigh could provide more reliable results. A model using complicated shapes and electrode positions may be a possibility as well, requiring considerable changes.

Improvements

To improve the method and balance the variance, more MUs need to be included in calibrating the model. This would also provide a much needed

error range for the depth estimation. Although it was difficult to find matching MUs in HDsEMG decomposition and iEMG, improvements in decomposition algorithms may provide enough MUs to reliable find matchings. Additionally, using decomposition of more iEMG electrodes could be an efficient way to calibrate the models.

There is a large amount of data in the HDsEMG recordings. Whilst all electrodes are used in decomposition and for extracting the MU potential distribution, the models neglects much of the data for depth estimation. Instead of only using the peak to peak values of the electrodes, other features like the energy of the signal could be explored as well. Expanding the models to cover more columns could reduce variance, making the results more reliable. Instead of applying a 1-dimensional gaussian fit to the data, a 2-dimensional surface could be used instead. Since the potential distribution is dependant on the fiber direction, a 2-dimensional fit could also be used for fibers in all directions.

For the two-layer model, adjusting the ratio of the attenuation powers in fat and muscle may be the flexibility the model needs to match the data. An additional layer, accounting for the skin should be considered as well. The issue that comes with increasing the amount of layers is that more unknown variables are introduced. Additional approximations will be required which may affect the results. Evaluating the level of detail best suited for the purpose is essential.

Clinical application

With more data and fine-tuning of the models, there are several ways to proceed with clinical application. For stroke rehabilitation, as mentioned in the introduction, it could give a measure for MU recovery by mapping MU activity to different muscles. It would serve as an additional assessment without impeding the patient's regular therapy. The patient would initially have the size of the relevant limb measured. Ultrasound measurements determine the thickness of the layers surrounding the muscle, i.e. the skin and fat layers. With these parameters the model is tailored for each patient. During standard rehabilitation exercises, HDsEMG measurements would be made, with a protocol and setup similar to the one in this thesis and

movements appropriate for the specific muscle. Many HDsEMG measurements need to be done over a certain time period to create a measure of MU recovery. With improved decomposition algorithms, more MUs can be mapped to different muscles. And with more data, the results will be more reliable. If necessary, a single parallel iEMG recording could be made to better calibrate the model in the initial phase when tailoring the model for the patient. From thereon only sEMG would be used, since the aim is to create a non-invasive method for MU localization.

Conclusion

Two models for depth estimation were provided. The direction of the results support the underlying theory, but there is high variance in the calibrated values for attenuation. More MUs are needed to create reliable models. Although the results are not conclusive, there is much that can be done to improve the models and move closer to clinical application.

References

(1) Roeleveld, K., Stegeman, D.F., Vingerhoets, H.M. and Oosterom, A.V., 1997. The motor unit potential distribution over the skin surface and its use in estimating the motor unit location. *Acta physiologica scandinavica*, *161*(4), pp.465-472.

(2) Widmaier, E.P., Raff, H., Strang, K.T. and Vander, A.J., 2008. *Vander's Human physiology: the mechanisms of body function*. Boston: McGraw-Hill Higher Education,.

(3) Peters, M.J., Stinstra, J.G. and Leveles, I., 2004. The electrical conductivity of living tissue: a parameter in the bioelectrical inverse problem. In *Modeling and imaging of bioelectrical activity* (pp. 281-319). Springer, Boston, MA.

(4) Vujaklija, I., Farina, D. and Aszmann, O.C., 2016. New developments in prosthetic arm systems. *Orthopedic research and reviews*, *8*, p.31.

(5) Hudgins, B., Parker, P. and Scott, R.N., 1993. A new strategy for multifunction myoelectric control. *IEEE Transactions on Biomedical Engineering*, *40*(1), pp.82-94.

(6) Jiang, N., Vest-Nielsen, J.L., Muceli, S. and Farina, D., 2012. EMG-based simultaneous and proportional estimation of wrist/hand kinematics in uni-lateral trans-radial amputees. *Journal of neuroengineering and rehabilitation*, *9*(1), p.42.

(7) Kapelner, T., Vujaklija, I., Jiang, N., Negro, F., Aszmann, O.C., Principe, J. and Farina, D., 2019. Predicting wrist kinematics from motor unit discharge timings for the control of active prostheses. *Journal of neuroengineering and rehabilitation*, *16*(1), p.47.

(8) Mackay, J. and Mensah, G.A., 2004. *The atlas of heart disease and stroke*. World Health Organization.

(9) Langhorne, P., Coupar, F. and Pollock, A., 2009. Motor recovery after stroke: a systematic review. *The Lancet Neurology*, *8*(8), pp.741-754.

(10) Langhorne, P., Bernhardt, J. and Kwakkel, G., 2011. Stroke rehabilitation. *The Lancet*, *377*(9778), pp.1693-1702.

(11) Gabriel, D.A., 2011. Effects of monopolar and bipolar electrode configurations on surface EMG spike analysis. *Medical*

engineering & physics, *33*(9), pp.1079-1085.

(12) Winter, D.A., Fuglevand, A.J. and Archer, S.E., 1994. Crosstalk in surface electromyography: theoretical and practical estimates. *Journal of Electromyography and Kinesiology*, *4*(1), pp.15-26.

(13) Ohashi, J., 1995. Difference in changes of surface EMG during low-level static contraction between monopolar and bipolar lead. *Applied Human Science*, *14*(2), pp.79-88.

(14) Negro, F., Muceli, S., Castronovo, A.M., Holobar, A. and Farina, D., 2016. Multi-channel intramuscular and surface EMG decomposition by convolutive blind source separation. *Journal of neural engineering*, *13*(2), p.026027.

(15) Kapelner, T., Negro, F., Aszmann, O.C. and Farina, D., 2017. Decoding motor unit activity from forearm muscles: perspectives for myoelectric control. *IEEE Transactions on Neural Systems and Rehabilitation Engineering*, *26*(1), pp.244-251.

(16) De Luca, C.J., Adam, A., Wotiz, R., Gilmore, L.D. and Nawab, S.H., 2006. Decomposition of surface EMG signals. *Journal of neurophysiology*, *96*(3), pp.1646-1657.

(17) Holobar, A. and Zazula, D., 2007, September. Gradient convolution kernel compensation applied to surface electromyograms. In *International Conference on Independent Component Analysis and Signal Separation* (pp. 617-624). Springer, Berlin, Heidelberg.

(18) Marco, G., Alberto, B. and Taian, V., 2017. Surface EMG and muscle fatigue: multi-channel approaches to the study of myoelectric manifestations of muscle fatigue. *Physiological measurement*, *38*(5), p.R27.

(19) Gabriel, S., Lau, R.W. and Gabriel, C., 1996. The dielectric properties of biological tissues: III. Parametric models for the dielectric spectrum of tissues. *Physics in Medicine & Biology*, *41*(11), p.2271.

Appendix 1

The MATLAB code of the first script, used to plot and extract MUs.

```
%samplingrate
S = 10240;

%Import Data, time and amplitude vectors
%Raw intramuscular EMG data
DataiEMG = load('CAiEMG.mat');
TimeiEMG = DataiEMG.Time;
DataiEMG = DataiEMG.Data;

%Raw surface EMG data
DatasEMG = load('CAsEMGx64_1110to1170.mat');
TimesEMG = DatasEMG.Time;                       %In seconds
DatasEMG = DatasEMG.Data;

%Motor unit firings, Decomponi data, Within DatasEMG range
Decomponi = load('Decomponi1110to1170.mat');
TimeDecomponi = Decomponi.Time;                 %In seconds
Decomponi = Decomponi.Data(:,7);

%%
%Choose column to fit a gaussian
col = 5;

%Window size to look for MU-firings
AvgWin1 = TimeDecomponi(1)+1;                           %Averaging
window start (s)
AvgWin2 = TimeDecomponi(end)-1;                         %Averaging
window end (s)

%Window size for each MU-firing
FireWin1 = -0.015;
       %Firing window start offset (s)
FireWin2 = 0.02;                                        %Firing
window end offset (s)

% Finds all MU-firings, adds them in seconds to FireTimings
AW1 = int64((AvgWin1-TimeDecomponi(1))*S);  %Conversion from sec
to index
AW2 = int64((AvgWin2-TimeDecomponi(1))*S);  %Conversion from sec
to index
FireTimings = [];
for i = AW1:AW2                                 %Finds MU-firings
within AvgWin
       if Decomponi(i) == 1
```

```
            FireTimings = [FireTimings TimeDecomponi(i)];
      End
end

% Sums all MU-firings, adds them to SumFirings
SumFirings = zeros(int64((FireWin2-FireWin1)*S),64);
SumiEMG = zeros(int64((0.01+0.01)*S));
%For each MU-firing
for i = 1:length(FireTimings)
      FW1 = int64((FireTimings(i)+FireWin1-TimesEMG(1))*S);
      FW2 = FW1 + length(SumFirings) - 1;

      %Raw sEMG within FireWin of MU-firing
      Firings = [];
      for j = 1:64
            Firings(:,j) = DatasEMG(FW1:FW2,j);
      end
      SumFirings = SumFirings + Firings;

end
%Average
AvgFirings = SumFirings/length(FireTimings);

%Min and Max for each sEMG
FireMax = max(AvgFirings);
FireMin = min(AvgFirings);

%Peak2Peak values for selected column
for j = 1:8
      ColP2P(j) = (FireMax(col+8*(j-1)) - FireMin(col+8*(j-1)));
End

%Vector with min P2P set to 0 to allow for gaussian fit
ColFit = ColP2P - min(ColP2P);

%P2P plot
figure
plot(ColFit)
title(['Average of ',num2str(length(FireTimings)),' MU-firings in
column ',num2str(col)])

%% iEMG and Decomponi plot
% Plots iEMG and MU-timings
figure
plot(TimeiEMG(AvgWin1*S:AvgWin2*S),DataiEMG(AvgWin1*S:AvgWin2*S))
hold on
plot(TimeDecomponi(AW1:AW2),Decomponi(AW1:AW2))
title([num2str(length(FireTimings)), ' MU-firings,
```

```
iEMG&Decomponi'])

%% Plots MU average over 64 sEMG plots
%Plots all 64 electrodes
figure
for j = 1:8
       for k = 1:8
              subplot(8,8,(j-1)*8+k)
              plot(AvgFirings(:,(j-1)*8+k))
              axis([0 length(AvgFirings) min(FireMin)
max(FireMax)]);
       end
end
```

Appendix 2

The MATLAB code of the second script, used to estimate and visualize the depth of the extracted MU.

```
%% Requires
% Column of P2P values, 'ColFit'
% Column, 'col'
% Average of firings for each electrode, 'AvgFirings'

%Circumference arm
Ca = 28;
%Radius arm
rA = Ca/2/pi;

%%Column variables
%Electrodes over skin
Li2 = [1 2 3 4 5 6 7 8];
%Gaussian fit of peak2peak values
GaussFitCol = fit(Li2',ColFit','Gauss1');
%Center of signal in the electrode vector
centerOfCol = GaussFitCol.b1;
% Shift electrode vector to align peak with 0
Li2 = Li2-centerOfCol;
%Electrode positions in radians
alphaLi2 = Li2/rA;
%Gaussian width constant of peak2peak fit
GaussWidth2 = GaussFitCol.c1;
%Full width at half maximum over skin
La2 = GaussWidth2*2*sqrt(log(2));
%Full width at half maximum in radians
alphaLa2 = La2/2/rA;

%% Main equation
%One-layer
%Set attenuation constant
Q2 = 1;
%These make writing the equation easier
gamma2 = 2^(-1/Q2);
c2 = 1-(1/gamma2)^2;
%Motor unit depth
d2 = rA/c2*((1-cos(alphaLa2))-sqrt((1-cos(alphaLa2)).^2-2*c2*(1-
cos(alphaLa2))))

%% Alternative equation
%Two-layer
%Set attenuation constants
Qmuscle = 0.5;
```

```
Qfat = Qmuscle*15;
%Fat thickness from ultrasound
Xfat = 0.3;

% System of equations
syms d rF
eqns = [(Qmuscle*(d-Xfat) + Qfat*Xfat)*(1-rF/d) == log(0.5), rA^2
+ (rA-d)^2 - 2*rA*(rA-d)*cos(alphaLa2) - rF^2 == 0, d>0, d<2*rA,
rF>0, rF<2*rA];
Solution = solve(eqns, [d rF]);

%Motor unit depth
d = double(Solution.d)
rF = double(Solution.rF);

%% Plot visualization of depth with column 'col'
%Arm outline
theta = linspace(0,pi,200);
%Plot fixed electrode positions (true) or fixed MU position
(false)
ElecPosFixed = true;

if ElecPosFixed == true
       ElecPos = [-3.5 -2.5 -1.5 -0.5 0.5 1.5 2.5 3.5];
else
       ElecPos = Li2;                                  %Electrode
positions
end

radius = Ca/2/pi;
depth = d2;

%Scaling factors for extracted motor units
x_scale = 0.5;
y_scale = 10;
plot_size = radius+1;

%Surface EMG from column 'col'
x_wave = [];
y_wave = [];
for i = 1:length(ElecPos)
       x_wave(:,i) = linspace(-x_scale,x_scale,length(AvgFirings))
- cos(ElecPos(i)/radius+pi/2)*radius*1.3;
       y_wave(:,i) = y_scale*AvgFirings(:,col+8*(i-1)) +
sin(ElecPos(i)/radius+pi/2)*radius*1.3;
end

%Electrode coordinates
```

```
x_elec = radius*-cos(ElecPos/radius+pi/2);
y_elec = radius*sin(ElecPos/radius+pi/2);
%MU coordinates
if ElecPosFixed == true
       x_MU = (radius-depth)*-cos((ElecPos(1)+centerOfCol-
1)/radius+pi/2);
       y_MU = (radius-depth)*sin((ElecPos(1)+centerOfCol-
1)/radius+pi/2);
else
       x_MU = 0;
       y_MU = radius-depth;
end

figure
hold on
plot(radius*cos(theta),radius*sin(theta),'k','LineWidth',4)
axis([-plot_size plot_size 0 1.5*plot_size])
pbaspect([1 0.75 1])
plot(x_elec,y_elec,'r.','MarkerSize',15)
plot(x_MU,y_MU,'ro','MarkerSize',7)
title(['Source depth = ',num2str(d2),' cm, Column
',num2str(col),', Center under
',num2str(centerOfCol)],'FontSize',12)
xlabel('cm')
ylabel('cm')
for i = 1:length(ElecPos)
       plot(x_wave(:,i),y_wave(:,i),'b')
end
```